Theoretical and experimental investigations on linear and nonlinear optical response of metal complexes doped PMMA films

2017 Mater. Res. Express 4 025024

(http://iopscience.iop.org/2053-1591/4/2/025024)

Materials Research Express

PAPER

RECEIVED
16 January 2017

REVISED
24 January 2017

ACCEPTED FOR PUBLICATION
30 January 2017

PUBLISHED
22 February 2017

Theoretical and experimental investigations on linear and nonlinear optical response of metal complexes doped PMMA films

P A Praveen[1], R Ramesh Babu[1] and K Ramamurthi[2]

[1] Crystal Growth and Thin Film Laboratory, Department of Physics, Bharathidasan University, Tiruchirappalli—620 024, Tamilnadu, India

[2] Crystal Growth and Thin Film Laboratory, Department of Physics and Nanotechnology, SRM University, Kattankulathur—603 203, Kancheepuram, Tamilnadu, India

E-mail: rampap2k@yahoo.co.in

Keywords: metal-organic complex, doped PMMA, semiempirical calculations, thermo-optic coefficient, Z-scan, optical limiting

Abstract

Metal organic complexes, diaceto bis benzimidazole cobalt(II) and diaceto bis benzimidazole copper(II), are synthesized by a simple chemical route. The synthesized powders are doped in PMMA with 1, 3, 5 wt% and deposited as free standing films of thickness $\sim$1 μm. For theoretical simulation, metal organic complex (MOC) embedded into the PMMA matrix is subjected to polarizability and hyperpolarizability calculations using the PM6 algorithm in MOPAC2012 package. It is found that the minimum interaction distance between PMMA and MOC is about 34 nm and does not vary with respect to the dopant. The copper complex shows higher interaction energy with the polymer matrix than the cobalt complex. Time dependent Hartree Fock approach is used to calculate the α, β and γ values for static, 0.25 and 0.5 eV energies; the cobalt complex shows higher polarizability and hyperpolarizability than the copper complex. Experimentally, the optical absorption, thermo-optic coefficient, nonlinear absorption coefficient and nonlinear refractive index of the samples are determined. The thermo-optic coefficients of the samples are seen to increase with increasing dopant concentration. From open aperture Z-scan studies the films are found to exhibit reverse saturable absorption behaviour, and from the closed aperture Z-scan all samples are found to exhibit self-focusing effects. The calculated third order susceptibility is in the order of 10^{-5} esu. The optical limiting properties are studied at 650 nm using a 20 mW laser and all the samples are found to exhibit good optical limiting in the operating wavelength.

1. Introduction

In the recent past, metal organic materials have been extensively investigated for their combined advantages of both organic and inorganic material properties [1]. For nonlinear optical considerations, the conjugated π-electron system of the organic moieties could respond rapidly to the applied field with large and extremely fast nonlinearities. On the other hand, metal ions in an organic medium often enhance the physical properties of the ligand such as thermal stability, mechanical durability and laser damage threshold. Metal ions in the complex will also induce additional electronic transitions, which is advantageous in the context of third order nonlinear optical applications [2]. Benzimidazole (BMZ), a heterocyclic aromatic compound, is well known for its anti-bacterial and anti-fungal activity [3]. For the last two decades it has attracted considerable interest in various sectors of material science, and many reports are available on BMZ and its derivatives for magnetic, gas adsorption, anti-corrosivity, anti-cancer, photophysical and photochemical applications [4–8]. Specifically, BMZ has been identified as a potential second harmonic generating (SHG) material, with a SHG efficiency 4.5 times better than that of KDP crystal [9]. There is a growing interest in the study of the coordination behaviour of BMZ with transition metal ions because of their improved properties—in particular, thin films of bis benzimidazole metal complexes show better nonlinear optical properties than those of BMZ thin films [10, 11]. In the synthesis of metal organic complexes (MOC), metal acetates as well as metal halides can be employed and the resulting product may contain either halide or acetate substituents depending on the coordination behaviour and type of reaction [12]. Computational studies show that these substituents play a significant role in polarizability

and hyperpolarizability of the molecule, and it is found that molecules with acetate substituents have better hyperpolarizability values than those with halide substituents [13]. But, experimentally, there are not many reports available on metal complexes of BMZ with acetate substituents especially in bis form. So, it is a matter of interest to synthesize and characterize BMZ metal complexes with acetate substituents. But treating BMZ with transition metal acetates often results rapid precipitation and the products are often not or very much less soluble in most solvents. So it is difficult to process the product further, as thin films or bulk crystals. Especially when considering materials for photonic applications, processing of nonlinear optical (NLO) material with specific requirements such as thickness and dimension is one of the important tasks for a researcher [14]. Like acetate substituted benzimidazole metal complexes, several materials are termed as having potential, but commercial interest is lacking due to their limitation in material processing for device fabrication [15]. For this reason, it is common to dope such materials into polymeric matrices to study their optical properties. In particular, low optical absorption characteristics at the operating wavelength and high sustainability are the key features for a good polymeric host [16]. Poly(methyl methacrylate) (PMMA) is one such polymer widely used as a host medium for the preparation of NLO composites. Several materials ranging from organic ligands, dyes, metal oxide nanostructures, inorganic composites were doped in the PMMA to obtain good NLO characteristics [17–19]. As part of our ongoing investigations on benzimidazole based metal complexes for nonlinear optical applications, we report in this paper on the theoretical and experimental studies of BMZ metal complex doped PMMA matrices. Semiempirical solid state calculations are used to model the NLO properties of the system based on guest–host interactions. The metal complexes are embedded into the PMMA matrix and their interaction energy and optical properties are modelled using the MOPAC2012 package with the PM6 algorithm. Further, the thermo-optic, third order nonlinear optical susceptibility and optical limiting properties of diaceto-bis-benzimidazole cobalt(II) (Co-BMZ) and diaceto-bis-benzimidazole copper(II) (Cu-BMZ) doped PMMA films are also reported.

2. Materials and methods

2.1. Synthesis of diaceto-bis-benzimidazole cobalt(II) and diaceto-bis-benzimidazole copper(II) complexes

All the raw materials used in the synthesis were reagent grade and purchased from Merck chemicals. The metal salts, cobalt acetate tetrahydrate ($Co(CH_3COO)_2(H_2O)_4$) and cupric acetate ($Cu(CH_3COO)_2$), were taken in 1:2 ratio with respect to the benzimidazole ligand. The metal salts and ligand were dissolved separately in ethanol. Then the ligand solution was added dropwise into the corresponding metal solution with stirring. Upon the continuous addition of the ligand solution, the cobalt solution turned from pink to violet colour and the copper solution from dark green to red. After a few minutes of stirring, violet coloured precipitate was obtained in the case of cobalt complex, whereas red precipitate was obtained in the case of copper complex. The synthesized materials were filtered, washed with double distilled water and dried in a hot air oven. To ensure the purity of the synthesized complexes, column chromatography was used. The product obtained was subjected to vibrational spectrum analysis to confirm the presence of functional groups. Figure 1 shows the recorded FTIR spectrum of Co-BMZ and Cu-BMZ complexes. The peaks observed at 424 cm^{-1} and 437 cm^{-1} in both spectra correspond to the metal–ligand vibration in the molecules [12]. Major changes observed in the ring modes of Co-BMZ and Cu-BMZ molecules with respect to their parent BMZ ligand could be attributed to the metal–nitrogen interaction. Presence of N–H vibrations at 1016 and 647 cm^{-1} in Co-BMZ, and 1112 and 647 cm^{-1} in Cu-BMZ indicate that the N–H bond of the imidazolate remains unaffected and the metal was coordinated through the molecule by the second N atom. Absorption peaks observed in the region 3600–2800 cm^{-1} of both spectra are due to the strong intermolecular hydrogen bonding between BMZ molecules in solid state. Figure 2 shows the proposed structure of the synthesized metal complexes.

2.2. Deposition of Co-BMZ and Cu-BMZ doped PMMA films

The Co-BMZ and Cu-BMZ doped PMMA films were prepared by dissolving 1 M of PMMA in chloroform and by adding the required amount of dopant (1, 3 and 5 wt%), either Co-BMZ or Cu-BMZ, into the solution. Then the prepared solution was transferred to a Teflon container and sonicated for 15 minutes. The clear polymeric solution obtained was cast on to a clean petri dish and dried well. After a few days, free standing films of the metal complex doped PMMA were scratched out from the glass plate. For comparison, undoped or pristine PMMA film was also deposited by a similar procedure. Due to the non-homogeneous dispersion of metal complexes in polymeric solution, we confined the doping level to within 5 wt%. The thickness of the deposited polymeric films were measured at about 1 micron; hereafter the pristine PMMA film is termed as PR and the other doped samples—Co-BMZ doped PMMA with 1, 3 and 5 wt% and Cu-BMZ doped PMMA with 1, 3 and 5 wt%—are termed as 1a, 3a, 5a and 1b, 3b, 5b respectively.

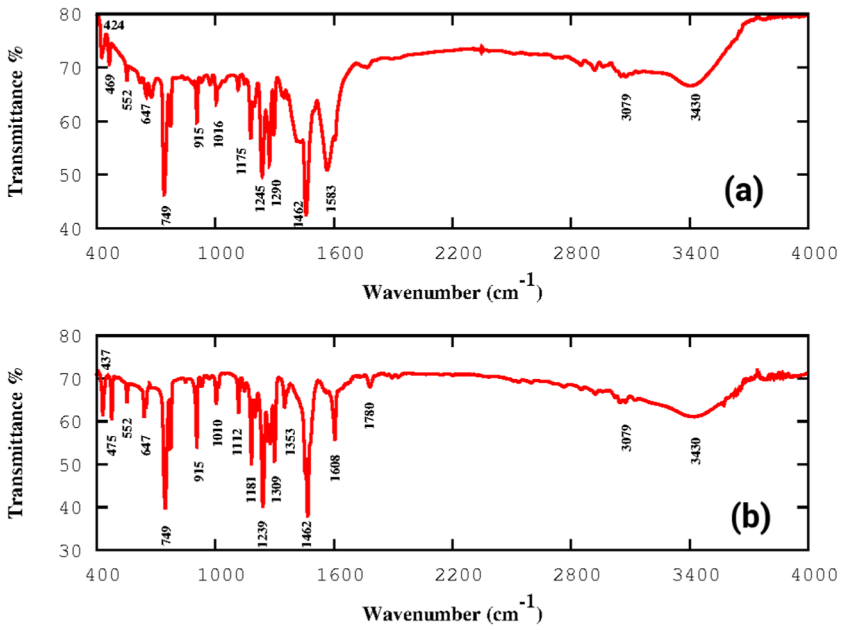

Figure 1. FT-IR spectrum of (a) Co-BMZ and (b) Cu-BMZ complexes.

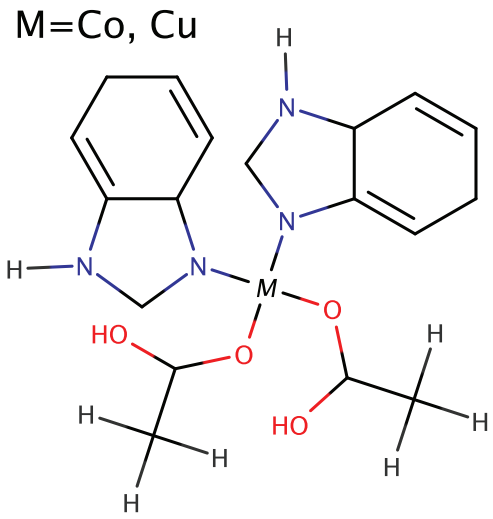

Figure 2. Structure of synthesized metal complexes.

2.3. Theoretical approach

Polymeric systems often consist of hundreds of atoms, and modelling their properties with theories like DFT will require considerable computational time. On the other hand, those sytems can be modelled with the help of less accurate classical treatments [20]. With the advent of new semiempirical methods such as PM6 and PM7, the feasibility of semiempirical calculations has been drastically increased. These modern methods provide better geometries and interaction energies for almost all the atoms in the periodic table [21, 22]. Even though it is possible to perform solid state calculations using semiempirical methods, only a very few attempts have been made in that area. In the present work, the PM6 algorithm in MOPAC2012 package has been used to model the solid state interactions between the benzimidazole metal complex and PMMA polymer matrix. Initially the structure of PMMA was drawn using Marvin Sketch package [23], and pre-optimized using the universal force field (UFF) algorithm available in the Avogadro package [24]. Then the molecule was optimized using the PM6 method in the MOPAC2012 package [25]. For solid state calculations, the MAKPOL program provided with MOPAC2012 was used to construct a polymer chain with 90 monomers. Similarly, the Co-BMZ and Cu-BMZ metal complex dopants were pre-optimized using UFF, and the molecular geometry further optimized using PM6. The structure obtained was embedded into the polymer system in the ratio of 90:1 (PMMA:MOC), and used in the simulations. For the energy gap calculation of metal complexes, the auxilary file of the optimized geometries was loaded into the Gabedit program and the highest occupied molecular orbital (HOMO) and the lowest unoccupied molecular orbital (LUMO) were estimated.

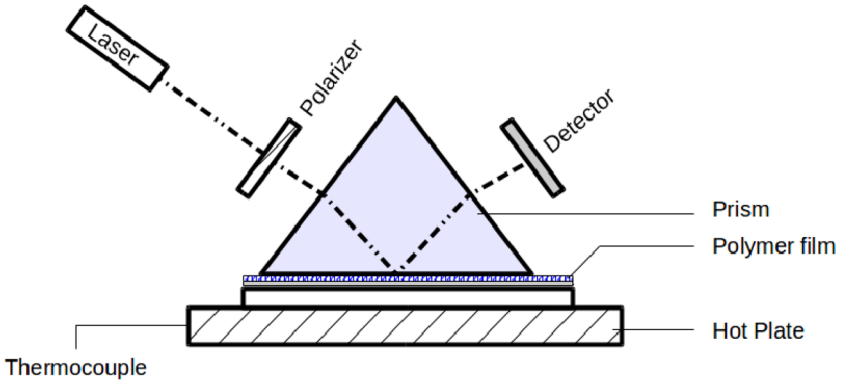

Figure 3. Schematic of experimental arrangement used to measure refractive index of the samples at different temperatures.

2.4. Characterization studies

The linear optical properties of the films were studied using a Perkin Elmer lambda UV-Vis. spectrometer in the wavelength range 300–800 nm. Figure 3 shows a schematic of the experimental setup used to determine the refractive index of PMMA and doped PMMA films at varying temperatures. The polymer film was placed on a substrate coated with silver paste and mounted on a hot-plate controlled by a temperature controller. The light beam from a diode laser of power 3 mW was passed through a polarizer to the interface between the prism and the glass substrate. The reflected light was detected using a photodiode. The entire setup was placed on a 360° rotating base with a vernier scale and adjustable to the desired angle. It is well known that when a polarized light wave is incident on the interface between two transparent media, the reflected wave entirely disappears at a particular angle of incidence known as the Brewster angle (θ_B) and the incident wave being totally transmitted into the second medium. By properly adjusting the rotating table, the value of θ_B can be determined, and from that value the refractive index of the polymer sample can be calculated. By measuring the refractive index at different temperatures, the thermo-optic coefficient of the sample can be calculated. Nonlinear optical properties of the films were studied using the Z-scan technique at room temperature. A CW diode laser of wavelength 650 nm and power 20 mW was used as the source. The beam of intensity about 7.8×10^8 W cm^{-2} was focused on to the sample using a lens of focal length 18 cm, and the sample was scanned along the z-axis with respect to the direction of propagation of the laser beam. Two types of configuration are possible in Z-scan by adjusting the aperture linear transmittance S. When $S = 1$, a configuration called open aperture (OA), the detector was insensitive to nonlinear refractive (NLR) effects. Therefore the nonlinear absorptive (NLA) effects can be evaluated using OA. In order to study the refractive effects, the second configuration— closed aperture (CA)—with 40% transmittance (S = 0.4) was used and the result divided by OA data to ensure the presence of complete NLR effects only. The optical limiting properties of the samples were studied by using a modified Z-scan setup [10]. A polarizer was placed in front of the lens to control the input power and the sample was mounted just after the focal point. Variation in output power with respect to the input was measured and plotted.

3. Results and discussion

3.1. Computational analysis

3.1.1. Interaction energy and energy gap analysis

The objective of the computational analysis is to investigate the interaction between the guest (MOC) and host (PMMA) and the corresponding variation in the NLO properties of the entire system. The location of MOC molecules in PMMA was visualized using the Molden program [26] and the acetate ion in the molecule was taken as the reference point to measure the distance between PMMA monomer and MOC. The smallest approachable distance between PMMA monomers and the MOC is about 34 nm, which differs slightly from previous molecular mechanics calculations [20]. This distance does not vary with respect to different dopants, since it is an intrinsic property of the polymer system. For interaction energy calculations, the entire system was optimized in two different conditions—one without any separation distance and the second with a separation distance about 100 nm between MOC and PMMA matrix. The interaction energy (ΔHf_{IE}) can be calculated using the relation [27],

$$\Delta Hf_{IE} = \Delta Hf_{Complex} - \Delta Hf_{Separate} \quad (1)$$

where $\Delta Hf_{Complex}$ is the heat of formation of the system without any separation distance and $\Delta Hf_{Separate}$ is the heat of formation of the system with MOC and PMMA matrix separated to a distance of 100 nm. The interaction energy between the MOC and PMMA matrix calculated using equation (1) is given in table 1. It can be seen that

Table 1. Interaction energy (Kcal mol^{-1}) of doped PMMA samples.

Molecule	$\Delta Hf_{\text{Separate}}$	$\Delta Hf_{\text{Complex}}$	ΔHf_{IE}
Co-BMZ	−247.25	−268.67	21.41
Cu-BMZ	−299.45	−334.50	35.04

Table 2. Calculated HOMO, LUMO and E_g values in atomic units.

Molecule	HOMO	LUMO	E_g
Co-BMZ	−0.2717	−0.07	0.2016
Cu-BMZ	−0.3037	−0.0155	0.2882

Table 3. Dipole moments of doped PMMA samples in Kcal mol^{-1}.

Molecule	*X*	*Y*	*Z*	Sum
Co-BMZ	0.33	7.74	0.44	7.76
Co-BMZ/PMMA	0.95	9.77	0.75	9.85
Cu-BMZ	1.01	3.81	0.19	3.95
Cu-BMZ/PMMA	1.43	5.06	−0.08	5.26

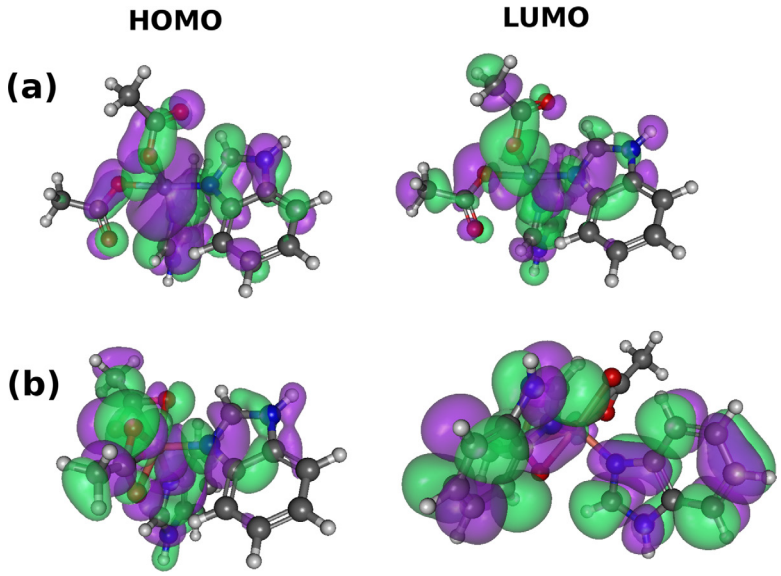

Figure 4. Frontier orbitals of Co-BMZ and Cu-BMZ molecules.

the interaction energy increases with respect to the metal ions, and the copper complex has more ΔHf_{IE} values than that of the cobalt complex. It is well known that lower interaction energy leads to higher mobility of the MOC inside the polymer matrix when it interacts with an applied field [28]. So, the values given in table 1 can be interpreted as indicating that Co-BMZ is more polarizable or readily polarizable than the Cu-BMZ complex. As further evidence for the role of metal ions in the interaction energy of polymeric systems, the estimated frontier orbitals, HOMO and LUMO (figure 4) are used to calculate the energy gap (E_g), and the results given in table 2. It can be seen that the Co-BMZ complex possesses lower energy gap values than the Cu-BMZ complex, which ensures the reliability of interaction energy calculations.

3.1.2. Dipole moments analysis

The necessity of dipole moment calculations is twofold. First, they can be used to estimate the polarizability of a system. Second, measuring dipole moments with and without the host can be useful to understanding the co-operative moments in the system. Considering co-operative moments, when doping a MOC in a polymer matrix of zero optical response, it is expected that the entire observed optical response from the system is the sum of the response from *N* individual MOCs, where *N* is an integer. So, the dipole moment of the system can be expressed as $\mu_{total} = N\mu$ [29]. But in certain instances there is a possibility of co-operative interactions between the MOCs and monomers, which may enhance the total optical response of the system. In such a scenario, the dipole moment of the system entirely depends on the number of bonded monomer units, and the enhancement

Table 4. Polarizability and hyperpolarizability values of PMMA composite in atomic units.

	α		β		$\gamma \times 10^3$	
Applied field (eV)	Co-BMZ	Cu-BMZ	Co-BMZ	Cu-BMZ	Co-BMZ	Cu-BMZ
0.0	307.71	267.88	1651.03	677.61	2686.95	44.66
0.25	308.22	268.15	1670.98	702.27	4494.56	47.85
0.5	309.77	268.96	1790.39	787.78	4668.25	61.32

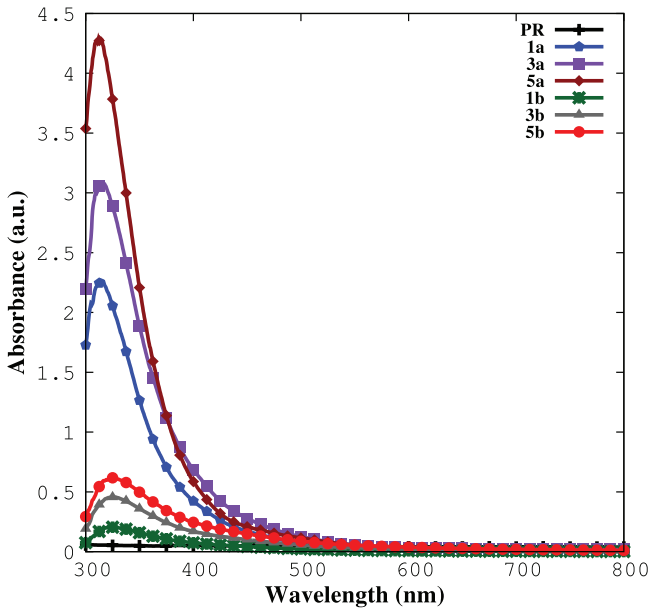

Figure 5. Absorption spectrum of pristine and doped PMMA samples.

in optical response can be attributed to the additional dipole moments arising from the monomers. So in the present work, the average dipole moment of the system was calculated from the MOPAC self-consistent field (SCF) calculation; the values calculated with and without PMMA are given in table 3. Higher dipole moments of Co-BMZ doped PMMA matrix indicate better potential of the system in optical applications. Further, the variation in dipole moments with and without PMMA suggests that the monomers around the metal complexes also tend to orient in the direction of the applied field, and this adds to the dipole moment of the entire system.

3.1.3. Polarizability and hyperpolarizability analysis

The efficiency of MOC doped PMMA matrices with respect to their NLO properties was studied by calculating the polarizability (α), first hyperpolarizability (β) and second hyperpolarizability (γ) values. For this purpose the COSMO (conductor like screening model) calculation was employed and electrostatic potential value for PMMA was taken as 2.7 (at 1 MHz). The calculations were carried out for static, 0.25 and 0.5 eV energies and the calculated α, β and γ values are given in table 4. It can be seen that the polarizability and hyperpolarizability values significantly increase with increase in the input energy. It is obvious that larger numbers of molecules tend to align in the applied field direction with increasing field strength. The Co-BMZ doped PMMA system shows better polarizability and hyperpolarizability values than the Cu-BMZ doped system; the higher values of Co-BMZ doped PMMA can be attributed to the contribution of unfilled d-shells in the Co-BMZ complex.

3.2. Linear absorption properties

Figure 5 shows the absorption spectrum of the pristine and doped PMMA samples. Both the complexes exhibit strong absorption between 300 and 400 nm, corresponding to intra-ligand transitions [30]. Optical scattering loss in the sample might induce absorption other than molecular absorption. But the very low absorption other than their characteristic molecular absorption in the visible window ensures the highly transparent nature and optical homogeneity of the samples. Minimum absorption at 650 nm is advantageous for nonlinear optical studies if the operational wavelength of the laser source is in that wavelength. So, one can expect higher order transitions rather than the linear electronic transitions. The variation in optical absorbance of the samples with respect to doping concentration indicates the direct influence of dopants in optical properties of the samples. Co-BMZ complex has higher linear absorption than the Cu-BMZ complex. Presence of spin–orbit coupling due to the unfilled d-shells of Co-BMZ (i.e. Cu-BMZ is more planar than the Co-BMZ) complex results more distortion in its tetrahedral geometry and it leads to the higher absorption [31].

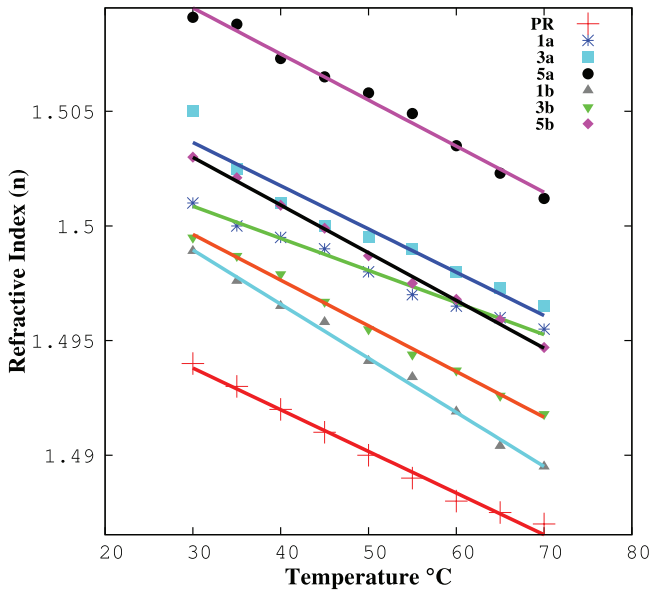

Figure 6. Variation of refractive index of the samples with respect to temperature.

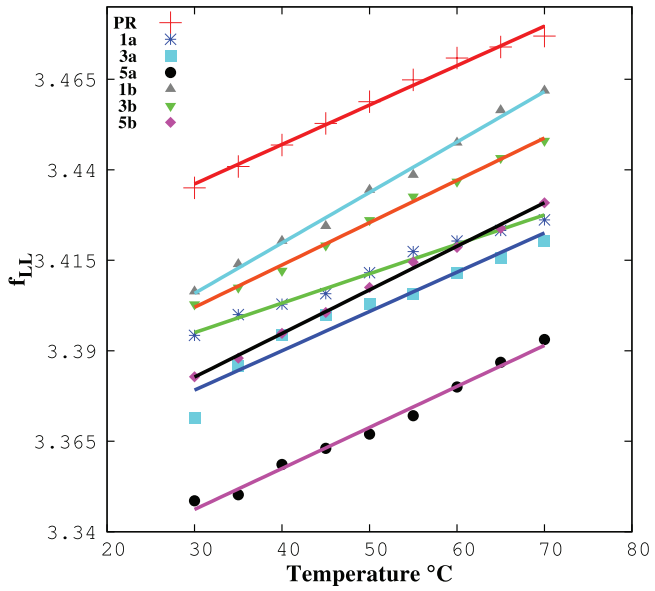

Figure 7. Calculated f_{LL} values with respect to temperature.

3.3. Thermo-optical coefficient

The thermo-optical experiment was performed using a transverse mode polarized laser and the measurements carried out in the cooling cycle, i.e. from 70 °C to 30 °C at a 5 °C interval for each measurement, in order to eliminate the possibility of moisture absorption in the samples. Since the glass transition temperature of PMMA is about 105 °C, a temperature range lower than that was chosen for the experiment. An additional advantage of opting for this range is that it is the working temperature range for most polymeric thermo-optic devices. The thermo-optic coefficient (TOC) of materials in terms of refractive index can be calculated using Prod'homme's theory as [32],

$$\frac{dn}{dT} = \frac{(n^2-1)(n^2+2)}{6n}(\phi - \beta_T) \tag{2}$$

where dn/dT is the TOC, n is the refractive index, ϕ is the temperature coefficient of the electronic polarizability and β_T is the thermal expansion coefficient. In the case of polymeric materials ϕ values are much lower than β_T values and TOC entirely depends on β_T. So, the equation (2) can be deduced as,

$$\frac{dn}{dT} = -\eta\beta_T \tag{3}$$

Table 5. Thermo-optical parameters of pristine and doped PMMA samples.

Sample	$\beta_T \times (10^{-4})/°C$	η	$\frac{dn}{dT} \times (10^{-4})°C$	f_{LL} of TM
PR	2.411	0.5816	−1.400	$T(8.1268\times10^{-4}) + 3.4034$
1a	3.201	0.5917	−1.816	$T(10.8516\times10^{-4}) + 3.7065$
3a	3.242	0.5974	−1.886	$T(10.8951\times10^{-4}) + 3.3465$
5a	3.419	0.6034	−2.010	$T(11.3274\times10^{-4}) + 3.3121$
1b	4.140	0.5886	−1.993	$T(11.6906\times10^{-4}) + 3.3669$
3b	3.472	0.5895	−2.080	$T(12.0367\times10^{-4}) + 3.3694$
5b	3.596	0.5946	−2.360	$T(13.9290\times10^{-4}) + 3.3640$

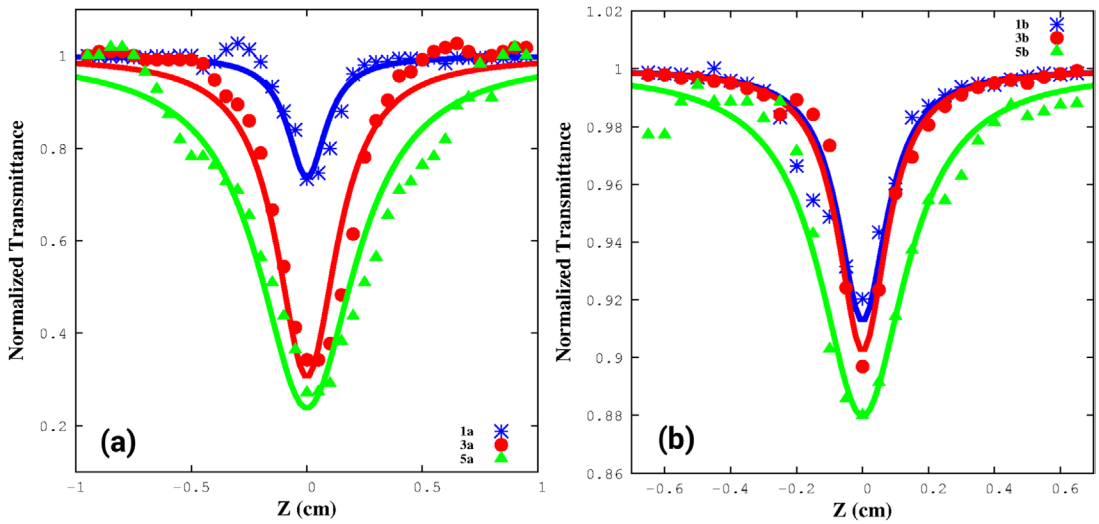

Figure 8. Open aperture Z-scan curves of (a) Co-BMZ and (b) Cu-BMZ doped PMMA samples.

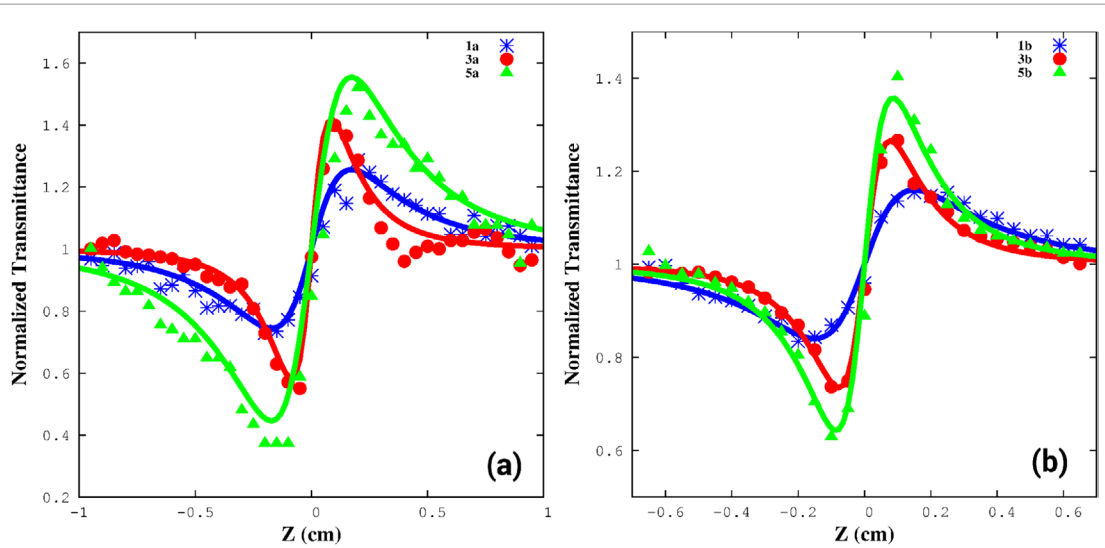

Figure 9. Closed aperture Z-scan curves of Co-BMZ and Cu-BMZ doped PMMA samples.

where,

$$\eta = \frac{(n^2-1)(n^2+2)}{6n} \tag{4}$$

According to Lorentz–Lorentz relation for the case of optical polymers, the function $\frac{(n^2-1)}{(n^2+2)}$ is proportional to the specific volume and appears as linear for different temperatures. From this, the thermal expansion coefficient β_T can be directly obtained as $\beta_T = a/b$ from the phenomenological expression [33],

Table 6. Third order nonlinear optical parameters of doped PMMA samples.

Sample	β (m w^{-1})	$n_2 \times 10^{-7}$ (m^2 w^{-1})	$\chi^{(3)} \times 10^{-5}$ esu	FOM (W)
1a	1.20	3.42	14.96	7.65
3a	3.19	4.59	26.34	7.93
5a	3.55	2.14	23.54	8.25
1b	0.39	1.31	5.56	3.24
3b	0.45	2.23	9.01	3.61
5b	0.54	2.94	11.81	3.83

$$f_{LL} = \frac{n^2 + 2}{n^2 - 1} = aT + b \tag{5}$$

where f_{LL} is a function corresponding to the variation of the Lorentz–Lorentz relation with respect to temperature, and a, b are the slope and intercept of the linear fit. By substituting the refractive index values measured for different temperatures (figure 6) in the above equation and the corresponding f_{LL} values were calculated and plotted (figure 7). The a and b values were derived from the linear fit of the data in figure 7 and from which the thermal expansion coefficient of the samples was calculated. Further, TOC was calculated by substituting the β_T in equation (3) and the calculated values are given in table 5. The TOC values obtained for the pristine PMMA sample are in agreement with previous reports, which ensures the reliability of the experiment [33]. It can be seen that the TOC and β_T values of Co-BMZ doped PMMA samples increases with increase in dopant percentage and in the case of Cu-BMZ doped PMMA samples, the values decrease and then increase. The thermo-optical property of the polymers is influenced by the sum of plasticization and thermal isomerization effects. Depending on the strength of a particular effect, the values of TOC and β_T can vary [33]. In the case of Co-BMZ doped samples, due to plasticization the thermal expansion coefficient of the samples is increased and a corresponding increase in TOC is observed. Since the Co-BMZ dopant favours the plasticization effect in the host, the β_T values increase with increasing dopant percentage. On the other hand, initially, Cu-BMZ dopant favours thermal isomerization and restricts the thermal expansion of the samples. But further increment in dopant percentage enhances the plasticization effect, and a corresponding variation is observed. An in-depth investigation is required to analyse the role of different dopants on the plasticization and thermal isomerization effect in polymers.

3.4. Third order nonlinear optical studies

The nonlinear optical properties of metal complex doped PMMA thin films were studied using a single beam Z-scan technique. Here the transmittance of the samples was measured with respect to sample position using a focused Gaussian profile laser beam. This simple method not only unravels the magnitude of the nonlinearity but also the sign of the nonlinear optical parameters. Thereby, the cause of nonlinearity can be easily interpreted. The present work is focused on employing a low power CW laser for measurements due to its potential application in the telecommunication wavelengths (to compensate the signal fluctuations) and for optical limiting (even a 5 mW laser pointer can damage human eyes) [34]. Figures 8 and 9 show the open and closed aperture Z-scan curves obtained for doped PMMA films, respectively. All the films were found to exhibit a valley-peak configuration corresponding to positive nonlinearity (i.e. self-focusing) in closed aperture scans. Reverse saturable absorption (RSA) behaviour of the films was observed from the open aperture (OA) scans. The RSA behaviour of doped PMMA thin films can be inferred with the help of five-level model [10]. Based on which the RSA behaviour of the samples is due to weak ground state absorption between $S_0 \rightarrow S_1$ followed by an intersystem crossing to T_1 energy level, then to a $T_1 \rightarrow T_2$ excited state absorption (ESA). RSA occurs at this wavelength because the excited state ($T_1 \rightarrow T_2$) absorption cross-section is larger than that of the ground state ($S_0 \rightarrow S_1$) absorption cross-section. There might be a possibility of two photon absorption (TPA) present in the samples, its contribution would further decrease the optical transition. But, since TPA is highly intensity dependent it is very much less likely to be produced in the CW regime. In the open aperture Z-scan, the absorption coefficient of the films can be related to transmittance using the relation [10]

$$T(Z) = 1 - \frac{q_0}{2\sqrt{2}\left(1 + \frac{z^2}{z_0^2}\right)} \tag{6}$$

where

$$q_0 = \beta I_0 L_{\text{eff}}, \tag{7}$$

I_0 is the intensity of the laser beam at focus ($z = 0$), L_{eff} is the effective thickness of the sample and can be calculated using the relation

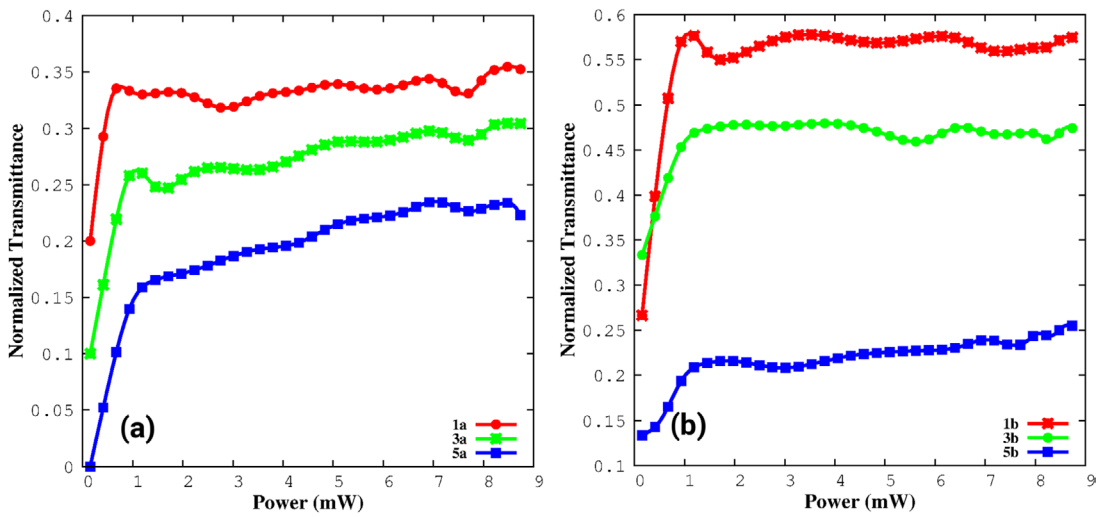

Figure 10. OL studies of (a) Co-BMZ and (b) Cu-BMZ doped PMMA samples.

$$L_{\text{eff}} = \frac{1 - e^{\alpha L}}{\alpha}. \tag{8}$$

Here L is the thickness of the film and α is the linear absorption coefficient of thin films and z_0 is the Rayleigh radius, could be obtained from the relation $z_0 = \pi\omega_0^2/\lambda$, where ω_0 is the beam waist and λ is the wavelength of source. The q_0 value was obtained by fitting the equation (6) to the experimental data and the β value was calculated by substituting back q_0 values in equation (7). For CA scans the nonlinear refractive index of the samples was calculated using the relation,

$$T(Z) = 1 - \frac{4\Delta\Phi.x}{(x^2+9)(x^2+1)} \tag{9}$$

where $x = z/z_0, \Delta\Phi$ is the laser induced phase shift and related to the nonlinear refractive index by the equation

$$n_2 = \frac{\Delta\Phi\lambda\alpha}{2\pi I_0(1 - e^{-\alpha l})} \tag{10}$$

Equation (9) is fitted to the experimental data to obtain $\Delta\Phi$ and by substituting back the value of $\Delta\Phi$ in equation (10), the n_2 value was calculated. The physical origin of nonlinear refraction could be electronic, molecular, electrostatic or thermal in nature. For doped PMMA films the major contribution may arise due to thermal effects, i.e. the energy of the focused light beam on the sample would induce heating in the medium and cause the appearance of a thermal gradient induced refractive index change that acts as a thermal lens and distorts the phase of a beam propagating through it [35]. This is one of the common phenomena observed in CW Z-scan studies. The nonlinear absorption and refractive coefficients were used to calculate the real ($\text{Re}\chi^{(3)}$) and imaginary ($\text{Im}\chi^{(3)}$) parts of third order nonlinear susceptibility ($\chi^{(3)}$) using the relations [10].

$$\text{Im}\chi^{(3)} = \frac{n^2\epsilon_0 C\lambda\beta}{2\pi} \tag{11}$$

and

$$\text{Re}\chi^{(3)} = 2n^2\epsilon_0 C n_2 \tag{12}$$

where C is the speed of light in vacuum, ϵ_0 is the free space permitivity and n is the linear refractive index of the material. The absolute values of third order nonlinear susceptibilities of doped PMMA films were calculated using,

$$|\chi^{(3)}| = [(\text{Re}\chi^{(3)})^2 + (\text{Im}\chi^{(3)})^2]^{1/2}. \tag{13}$$

The calculated nonlinear optical parameters are listed in table 6. The order of magnitude of $\chi^{(3)}$ is about 10^{-5} esu. Also, the imaginary part of $\chi^{(3)}$ is significantly larger than the real part, meaning that the nonlinear absorption is the dominant mechanism in the samples. The β, n_2 and $\chi^{(3)}$ values increase with increasing dopant concentration. This can be interpreted as the direct influence of dopants in third order nonlinear optical properties of the doped PMMA samples. The figure of merit of the samples were calculated using the relation $W = \Delta.n/\alpha\lambda$ and for a device quality sample it is essential to achieve $|W| \gg 1$ [36]. For doped PMMA films, the values (table 6) satisfy the above condition and ensures the versatility of the samples towards optical applications. Figure 10 shows the optical

limiting (OL) behaviour of the doped PMMA films. At low input powers, the output intensity increases linearly with it. But at higher irradiance the nonlinear medium starts to limit the output intensity, which clamps at a certain power. The limiting ability of the sample increases with increase in dopant concentration. Of the two dopants, Co-BMZ doped PMMA samples show better limiting behaviour than Cu-BMZ doped samples. This can be interpreted with the help of OA Z-scan curves. Due to the high nonlinear absorption in the samples a better OL is achieved.

4. Conclusions

Co-BMZ and Cu-BMZ complexes were prepared by a simple chemical route and doped into a PMMA matrix with different weight percentages. From computational studies, the location of the MOC in PMMA matrix was found to be an intrinsic property of a polymer, and the distance between the dopants and polymer matrix not to be affected by the nature of the dopant. Interaction energy calculation reveals that the cobalt complex is more polarizable than the copper complex, and co-operative dipole moments calculations indicate the positive response of PMMA monomers towards the applied field. From the theoretically calculated optical properties, it was found that the cobalt complex shows better polarizability and hyperpolarizability than the copper complex. Further, the samples were studied in regard to their thermo-optic and nonlinear optical properties. Due to their distorted tetragonal geometry, Co-BMZ samples showed a higher linear absorption than the Cu-BMZ samples. The thermo-optic coefficient was found to vary with respect to the dopant concentration due to the plasticization and thermal isomerization effect. Since the Co-BMZ samples favoured plasticization, their TOC and β_T values increased with increasing dopant concentration. Conversely, in the case of Cu-BMZ samples, at lower dopant percentage the system favours thermal isomerization, but increasing dopant percentage leads to a increase in thermal expansion coefficient. Thermally induced self-focusing and reverse saturable effects were observed in the third order nonlinear optical studies of the samples. The third order susceptibility was of the order of 10^{-5} esu. The high figure of merit of the samples ensures the potential of Co-BMZ and Cu-BMZ doped PMMA films for future photonic applications.

Acknowledgments

Authors acknowledge the financial assistance from School of Physics, Bharathidasan University, provided by DST-FIST (Order No: SR/FIST/PSI-204/2015 (c)) for the establishment of research facilities. Further, one of the authors PA Praveen thank the UGC-BSR Govt. of India for financial assistance in the form of 'Research Fellowship in Science for Meritorious Students' (F.4-1/2006/7-197/2007(BSR)).

References

[1] Ding R, Huang C, Lu J, Wang J, Song C, Wu J, Hou H and Fan Y 2015 Solvent templates induced porous metal–organic materials: Conformational isomerism and catalytic activity *Inorg. Chem.* **54** 1405–13
[2] Carne A, Carbonell C, Imaz I and Maspoch D 2011 Nanoscale metal–organic materials *Chem. Soc. Rev.* **40** 291–305
[3] Kim H J, Heo C H and Kim H M 2013 Benzimidazole-based ratiometric two-photon fluorescent probes for acidic ph in live cells and tissues *J. Am. Chem. Soc.* **135** 17969–77
[4] Bahrami F, Panahi F, Daneshgar F, Yousefi R, Shahsavani M B and Khalafi-Nezhad A 2016 Synthesis of new α-aminophosphonate derivatives incorporating benzimidazole, theophylline and adenine nucleobases using l-cysteine functionalized magnetic nanoparticles (lcmnp) as magnetic reusable catalyst: evaluation of their anticancer properties *RSC Adv.* **6** 5915–24
[5] Ashourirad B, Sekizkardes A K, Altarawneh S and El-Kaderi H M 2015 Exceptional gas adsorption properties by nitrogen-doped porous carbons derived from benzimidazole-linked polymers *Chem. Mater.* **27** 1349–58
[6] Tang Y, Zhang F, Hu S, Cao Z, Wu Z and Jing W 2013 Novel benzimidazole derivatives as corrosion inhibitors of mild steel in the acidic media. Part I: gravimetric, electrochemical, sem and xps studies *Corros. Sci.* **74** 271–82
[7] Łukowska-Chojnacka E, Wińska P, Wielechowska M, Poprzeczko M and Bretner M 2016 Synthesis of novel polybrominated benzimidazole derivatives-potential ck2 inhibitors with anticancer and proapoptotic activity *Bioorganic Med. Chem.* **24** 735–41
[8] Tayade R P and Sekar N 2016 Benzimidazole-thiazole based nlophoric styryl dyes with solid state emission–synthesis, photophysical, hyperpolarizability and td-dft studies *Dyes Pigments* **128** 111–23
[9] Krishna A, Vijayan N, Bagdia C, Thukral K, Haranath D, Maurya K K and Bhagavannarayana G 2016 Effect of ampoule support on the growth of organic benzimidazole single crystals by vertical bridgman technique for nonlinear optical applications *CrystEngComm* **18** 4844–50
[10] Praveen P A, Ramesh Babu R, Jothivenkatachalam K and Ramamurthi K 2015 Spectral, morphological, linear and nonlinear optical properties of nanostructured benzimidazole metal complex thin films *Spectrochim. Acta* A **150** 280–89
[11] Praveen P A, Ramesh Babu R and Ramamurthi K 2017 Role of annealing on the structural and optical properties of nanostructured diaceto bis-benzimidazole mn(ii) complex thin films *Spectrochim. Acta* A **173** 800–08
[12] Şahin E, Ide S, Kurt M and Yurdakul Ş 2002 Structural investigation of dibromobis (benzimidazole) zn (ii) complex *J. Mol. Struct.* **616** 259–64
[13] Praveen P A and Ramesh Babu R 2016 Effect of substituents on polarizability and hyperpolarizability values of benzimidazole metal complexes *AIP Conf. Proc.* **1731** 090013
[14] Bosshard C, Hulliger J, Florsheimer M and Gunter P 2001 *Organic Nonlinear Optical Materials* (Boca Raton, FL: CRC Press)
[15] Sugioka K and Cheng Y 2014 Ultrafast lasers-reliable tools for advanced materials processing *Light: Sci. Appl.* **3** e149

[16] Spiridon M C, Iliopoulos K, Jerca F A, Jerca V V, Vuluga D M, Vasilescu D S, Gindre D and Sahraoui B 2015 Novel pendant azobenzene/polymer systems for second harmonic generation and optical data storage *Dyes Pigments* **114** 24–32
[17] Tao L, Long H, Zhou B, Yu S F, Lau S P, Chai Y, Fung K H, Tsang Y H, Yao J and Xu D 2014 Preparation and characterization of few-layer mos 2 nanosheets and their good nonlinear optical responses in the pmma matrix *Nanoscale* **6** 9713–9
[18] Wu W-J, He W-L, Yu H-Yu, Huang H-X, Chen M and Qian D-J 2017 Synthesis and photophysical properties of pyrene-functionalized nano-sio 2 hybrids in solutions and doped-pmma thin films *Mater. Chem. Phys.* **186** 179–87
[19] Lyutakov O, Goncharova I, Rimpelova S, Kolarova K, Svanda J and Svorcik V 2015 Silver release and antimicrobial properties of pmma films doped with silver ions, nano-particles and complexes *Mater. Sci. Eng.* C **49** 534–40
[20] Makowska-Janusik M and Benard J F 2007 Determination of the macroscopic optical properties for composite materials *J. Phys.: Conf. Ser.* **79** 012030
[21] Praveen P A, Ramesh Babu R and Ramamurthi K 2015 Validation of pm6 & pm7 semiempirical methods on polarizability calculations *AIP Conf. Proc.* **1665** 090011
[22] Kinal A and Sayhan S 2016 Accurate prediction of hydrogen storage capacity of small boron nitride nanocages by dispersion corrected semi-empirical pm6-dh2 method *Int. J. Hydrog. Energy* **41** 392–400
[23] Csizmadia P 1999 Marvinsketch and marvinview: molecule applets for the world wide web *Proc. of The 3rd Int. Electronic Conf. on Synthetic Organic Chemistry* vol **1** pp 367–9
[24] Hanwell M D, Curtis D E, Lonie D C, Vandermeersch T, Zurek E and Hutchison G R 2012 Avogadro: an advanced semantic chemical editor, visualization, and analysis platform *J. Cheminformatics* **4** 17
[25] Stewart J J P 2004 Optimization of parameters for semiempirical methods iv: extension of mndo, am1, and pm3 to more main group elements *J. Mol. Model.* **10** 155–64
[26] Schaftenaar G and Noordik J H 2000 Molden: a pre-and post-processing program for molecular and electronic structures *J. Comput.-Aided Mol. Des.* **14** 123–34
[27] Muddana H S and Gilson M K 2012 Calculation of host-guest binding affinities using a quantum-mechanical energy model *J. Chem. Theory Comput.* **8** 2023–33
[28] Sidhu L S, Halder A and Rai S 2016 Dopant induced modulation in the structure and electronic properties of au 10 cluster *RSC Adv.* **6** 87115–23
[29] Minkin V I 2012 *Dipole Moments in Organic Chemistry* (Berlin: Springer)
[30] Zadrozny J M, Telser J and Long J R 2013 Slow magnetic relaxation in the tetrahedral cobalt (ii) complexes (co (eph) 4) 2-(e o, s, se) *Polyhedron* **64** 209–17
[31] Hitchman M A 1977 Electronic structure of low-spin cobalt(ii) schiff base complexes *Inorg. Chem.* **16** 1985–93
[32] Kang E-S, Lee T-H and Bae B-S 2002 Measurement of the thermo-optic coefficients in sol-gel derived inorganic–organic hybrid material films *Appl. Phys. Lett.* **81** 1438–40
[33] Li X, Cao Z, Shen Q and Yang Y 2006 Influence of dopant concentration on thermo-optic properties of pmma composite *Mater. Lett.* **60** 1238–41
[34] Innocenzi P and Lebeau B 2005 Organic–inorganic hybrid materials for non-linear optics *J. Mater. Chem.* **15** 3821–31
[35] Godin T, Moncorgé R, Doualan J-L, Fromager M, Ait-Ameur K, Cruz R A and Catunda T 2012 Optically pump-induced athermal and nonresonant refractive index changes in the reference cr-doped laser materials: Cr: Gsgg and ruby *J. Opt. Soc. Am.* B **29** 1055–64
[36] Zafar S, Khan Z H and Khan M S 2014 Study of self-defocusing, reverse saturable absorption and photoluminescence in anthraquinone PMMA nanocomposite film *Spectrochim. Acta* A **118** 852–6